bioRxiv preprint doi: https://doi.org/10.1101/834614; this version posted December 16, 2019. The copyright holder for this preprint (which was not certified by peer review) is the author/funder, who has granted bioRxiv a license to display the preprint in perpetuity. It is made available under aCC-BY-NC-ND 4.0 International license.

Boosting Brain Signal Variability Underlies Liberal Shifts in Decision Bias

Niels A. Kloosterman[1,2*], Julian Q. Kosciessa[1,2], Ulman Lindenberger[1,2], Johannes Jacobus Fahrenfort[3], Douglas D. Garrett[1,2]

[1]Max Planck UCL Centre for Computational Psychiatry and Ageing Research and [2]Center for Lifespan Psychology, Max Planck Institute for Human Development, Lentzeallee 94, 14195 Berlin, Germany

[3]Department of Experimental and Applied Psychology, Vrije Universiteit, van der Boechorststraat 1, 1081 BT Amsterdam, The Netherlands

[4]Department of Psychology, University of Amsterdam, The Netherlands;

*Correspondence: Niels Kloosterman

Email: kloosterman@mpib-berlin.mpg.de

Author ORCIDs

Niels A Kloosterman http://orcid.org/0000-0002-1134-7996
Julian Kosciessa https://orcid.org/0000-0002-4553-2794
Ulman Lindenberger https://orcid.org/0000-0001-8428-6453
Johannes Jacobus Fahrenfort http://orcid.org/0000-0002-9025-3436
Douglas D Garrett https://orcid.org/0000-0002-0629-7672

Classification

Biological Sciences / Neuroscience

Keywords

Brain signal variability, decision bias, perceptual decision making, signal detection theory, flexibility

Author Contributions

Niels Kloosterman, Conceptualization, Data curation, Software, Formal analysis, Investigation, Visualization, Methodology, Writing—original draft, Project administration, Writing—review and editing; Julian Kosciessa, Software, Formal analysis, Writing—review and editing; Ulman Lindenberger, Resources, Funding acquisition, Writing—review and editing; Johannes Jacobus Fahrenfort, Conceptualization, Data curation, Software, Formal analysis, Supervision, Visualization, Methodology, Writing—original draft, Project administration, Writing—review and editing; Douglas Garrett, Conceptualization, Resources, Formal analysis, Supervision, Funding acquisition, Investigation, Methodology, Writing—review and editing.

bioRxiv preprint doi: https://doi.org/10.1101/834614; this version posted December 16, 2019. The copyright holder for this preprint (which was not certified by peer review) is the author/funder, who has granted bioRxiv a license to display the preprint in perpetuity. It is made available under aCC-BY-NC-ND 4.0 International license.

Abstract

Strategically adopting decision biases allows organisms to tailor their choices to environmental demands. For example, a liberal response strategy pays off when target detection is crucial, whereas a conservative strategy is optimal for avoiding false alarms. Implementing strategic bias shifts is presumed to rely on prefrontal cortex, but human evidence for this is scarce. We hypothesized that strategic liberal bias shifts during a continuous target detection task arise through a more unconstrained neural regime (higher entropy) suited to the detection of unpredictable events. Upregulation of entropy in frontal brain regions indeed strongly characterized the degree to which individuals shifted from a conservative to a liberal bias. EEG standard deviation and spectral power could not account for this relationship, highlighting the unique contribution of moment-to-moment neural variability to bias shifts. Modulation of neural variability through prefrontal cortex appears instrumental for permitting an organism to tailor its decision bias to environmental demands.

Impact statement

Moment-to-moment variability is a prominent feature of neural activity. Rather than representing mere noise, this variability might enable us to flexibly adapt our decision biases to the environment.

Introduction

We often reach decisions not only by objectively weighing different alternatives, but also by allowing subjective decision biases to influence our choices. Ideally, such biases should be under internal control, allowing us to flexibly adapt to changes in task context while performing a challenging task. Specifically, contexts which prioritize target detection benefit from a liberal response strategy, whereas a conservative strategy should be used at times when it is important to avoid errors of commission (e.g., false alarms). Strategic shifts in decision bias are presumed to rely on prefrontal cortex (Rahnev et al., 2016), but despite growing interest (Chen et al., 2015; Reckless et al., 2014; Windmann et al., 2002), the spatio-temporal neural signature of such within-person bias shifts is unknown. As such, how strategic decision biases are neuronally implemented and retained during a specific task context remain open questions.

One candidate neural signature of decision bias shifts that has not been considered thus far is moment-to-moment variability of brain activity. Temporal neural variability is a prominent feature in all types of neural recordings (single-cell, local field potentials, EEG/MEG, fMRI), which has traditionally been considered ‘noise’ that corrupts neural computations. However, increasing evidence suggests that temporal variability can instead prove optimal for neural systems, allowing individuals to perform better, respond faster, and adapt quicker to their environment (Garrett et al., 2015, 2013, 2011). Here, we perform a crucial test of the utility of

bioRxiv preprint doi: https://doi.org/10.1101/834614; this version posted December 16, 2019. The copyright holder for this preprint (which was not certified by peer review) is the author/funder, who has granted bioRxiv a license to display the preprint in perpetuity. It is made available under aCC-BY-NC-ND 4.0 International license.

moment-to-moment neural variability in the context of adaptive human decision making. We hypothesized that within-person upregulation of neural variability would implement a strategic, liberal bias shift that 'opens up' the decision-making process more widely to target input from the environment (Marzen and DeDeo, 2017; Młynarski and Hermundstad, 2018). Specifically, we reasoned that increased neural variability might underlie a state of higher receptiveness to, and preparedness for, events of interest that occur at unpredictable moments in time, thus allowing the decision maker to adopt a more liberal bias towards deciding that such an event has indeed occurred.

We tested this hypothesis using data from humans performing a challenging, continuous target detection task under two different decision bias manipulations, while non-invasively recording their electroencephalogram (EEG) (Kloosterman et al., 2019). Sixteen participants (three experimental sessions each) were asked to detect orientation-defined squares within a continuous stream of line textures of various orientations and report targets via a button press (Figure 1A). In alternating nine-minute blocks of trials, we actively biased participants' perceptual decisions by instructing them either to report as many targets as possible (liberal condition), or to only report high-certainty targets (conservative condition). We played auditory feedback after errors and imposed monetary penalties to enforce instructions.

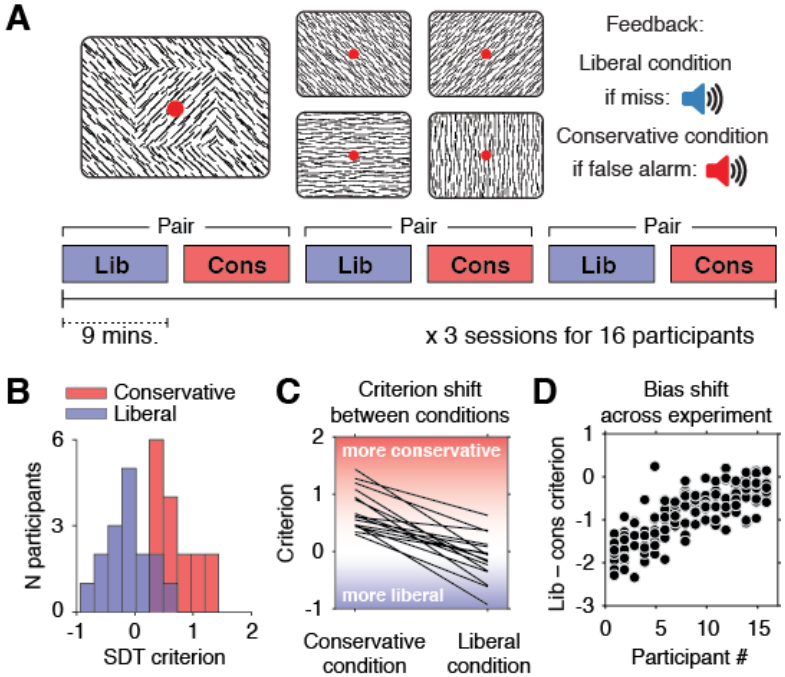

Figure 1 | **Experimental paradigm and behavioral results A.** Top, target and non-target stimuli. Subjects detected targets (left panel) within a continuous stream of diagonal and cardinal line stimuli (middle panel), and reported targets via a button press. In different blocks of trials, subjects were instructed to actively avoid either target misses (liberal condition) or false alarms (conservative condition). Auditory feedback was played directly after the respective error in both conditions (right panel). Bottom, time course of an experimental session. The two conditions were alternatingly administered in blocks of nine minutes. In between blocks participants were informed about current task performance and received instructions for the next block. Subsequent liberal and conservative

bioRxiv preprint doi: https://doi.org/10.1101/834614; this version posted December 16, 2019. The copyright holder for this preprint (which was not certified by peer review) is the author/funder, who has granted bioRxiv a license to display the preprint in perpetuity. It is made available under aCC-BY-NC-ND 4.0 International license.

blocks were paired for within-participant analyses (see panel D, and Figure 3C). **B.** Distributions of participants' criterion in both conditions. A positive criterion indicates a more conservative bias, whereas a negative criterion indicates a more liberal bias. **C.** Corresponding within-person slopes. **D.** Within-person bias shifts for liberal–conservative block pairs (see panel A, bottom). Participants were sorted based on average criterion shift before plotting.

The following figure supplement is available for Figure 1:

Figure supplement 1 | Perceptual sensitivity and relationship between decision bias and sensitivity.

In our previous paper on these data, we reported within-participant evidence that decision bias in each condition separately is implemented by modulating the accumulation of sensory evidence in posterior brain regions through oscillatory EEG activity in the 8-12 Hz (alpha) and gamma (60-100 Hz) frequency ranges (Kloosterman et al., 2019). In no brain region, however, did we find a change-change relationship between participants' liberal–conservative shifts in decision bias and in spectral power, despite substantial available data (on average 1733 trials per participant) and considerable individual differences in the bias shift. Reasoning that moment-to-moment variability of neural activity may instead better capture the bias shift from person to person and possibly reveal its hypothesized prefrontal signature, we here measured temporal variability in the EEG data using a novel algorithm based on multi-scale entropy (MSE)(Costa et al., 2002). We then tested for a change-change relationship by correlating within-person liberal–conservative shifts in decision bias with those estimated via our modified MSE (mMSE) measure. Furthermore, we explicitly investigated the unique contribution of moment-to-moment neural variability to the bias shift by statistically controlling for the standard deviation and spectral power of the EEG signal. Finally, following a different line of literature, previous work has also linked a transient variability reduction (referred to as 'quenching') to improved cognitive ability (Arazi et al., 2017; Churchland et al., 2010; Schurger et al., 2015). We examined whether a transient variability reduction also occurs in entropy and to what extent it is related to behavior in our task.

Results

Participants differentially adopted the intended decision biases in the respective conditions, as quantified by the criterion measure from signal detection theory (SDT) (Green and Swets, 1966). Subjects assumed a lower criterion (more liberal bias) when target detection was emphasized (c = –0.13, standard deviation (SD) 0.4) and adopted a higher criterion (more conservative bias) when instructed to avoid false alarms (c = 0.73, SD 0.36; liberal vs. conservative, p = 0.001, two-sided permutation test, 10,000 permutations)(Figure 1B). Participants varied substantially not only in the average criterion they used across the two conditions (range of c = –0.24 to 0.89), but also in the size of the criterion shift between conditions (range of Δc = –1.54 to –0.23). Highlighting the extent of individual differences, participant's biases in the two conditions were only weakly correlated (Spearman's rho = 0.24, p = 0.36), as can be seen from the subjects' large variation in criterion intercept and slope between the two conditions in Figure 1C. Moreover, the bias shift also fluctuated to some extent within participants over the course of the experiment, as indicated by

bioRxiv preprint doi: https://doi.org/10.1101/834614; this version posted December 16, 2019. The copyright holder for this preprint (which was not certified by peer review) is the author/funder, who has granted bioRxiv a license to display the preprint in perpetuity. It is made available under aCC-BY-NC-ND 4.0 International license.

variation in criterion differences between successive, nine-minute liberal and conservative blocks (participant-average SD 0.37, Figure 1D). Participants also varied widely in their ability to detect targets (range in SDT d` 0.26 to 3.97), but achieved similar d` in both bias conditions (rho = 0.97, $p < 0.001$, Figure 1, figure supplement 1). Moreover, the liberal–conservative bias shift was only weakly correlated with a shift in sensitivity across participants (rho = 0.44, $p = 0.09$), indicating that the bias manipulation largely left perceptual sensitivity unaffected. In our previous paper on these data (Kloosterman et al., 2019), we also quantified decision bias in terms of the 'drift bias' parameter within the drift diffusion model (Ratcliff and McKoon, 2008). We chose to focus on SDT criterion in the current paper due to its predominant use in the literature and its comparably simpler computation, while noting the substantial overlap between the two measures as indicated by their high correlation (rho = –0.89, as reported in our previous paper). Taken together, we observed considerable variability in strategic decision bias shifts as a result of our bias manipulation, both at the group level and within single individuals.

We exploited the between- and within-participant variations in liberal–conservative criterion differences to test our hypothesis that a boost in brain signal variability underlies a liberal bias shift. To this end, we developed a novel algorithm based on multi-scale entropy (MSE) that directly quantifies the temporal irregularity of the EEG signal at longer and shorter timescales by counting how often temporal patterns in the signal reoccur during the signal's time course (Costa et al., 2002)(Figure 2A, bottom). In general, signals that tend to repeat themselves over time, such as neural oscillations, are assigned lower entropy, whereas more irregular, non-repeating signals yield higher entropy. We developed time-resolved, modified MSE (mMSE), that differs from traditional MSE in two ways. First, slower timescales are usually assessed by 'coarsegraining' the data by means of averaging of neighboring data samples and repeating the pattern counting operation depicted in Figure 2A. Although this method can remove faster dynamics from the data in a simple way, it is prone to aliasing artifacts and thereby possibly obscures genuine entropy effects in the data. Therefore, we instead coarsegrain the data using a Butterworth low-pass filter, followed by skipping of data points to coarsen the data (Figure 2B), thereby retaining better control over the frequencies present in the coarse-grained signal (Semmlow, 2004; Valencia et al., 2009). Second, conventional entropy analysis requires substantial continuous data (in the order of minutes) for robust estimation, which makes the standard method unsuitable for studying brief, transient cognitive processes such as decision-making. To investigate entropy dynamics over time, we calculated entropy across discontinuous data segments aggregated across trials via a sliding window approach (Grandy et al., 2016) (Figure 2A, top). Prior to mMSE analysis, we removed stimulus-evoked EEG activity by subtracting the event-related potential (computed by averaging all trials within a condition), from each single trial. This was done to focus on ongoing neural activity

bioRxiv preprint doi: https://doi.org/10.1101/834614; this version posted December 16, 2019. The copyright holder for this preprint (which was not certified by peer review) is the author/funder, who has granted bioRxiv a license to display the preprint in perpetuity. It is made available under aCC-BY-NC-ND 4.0 International license.

(Klimesch et al., 1998). Please see Materials and Methods for details on the various analysis steps and our modifications of the MSE algorithm.

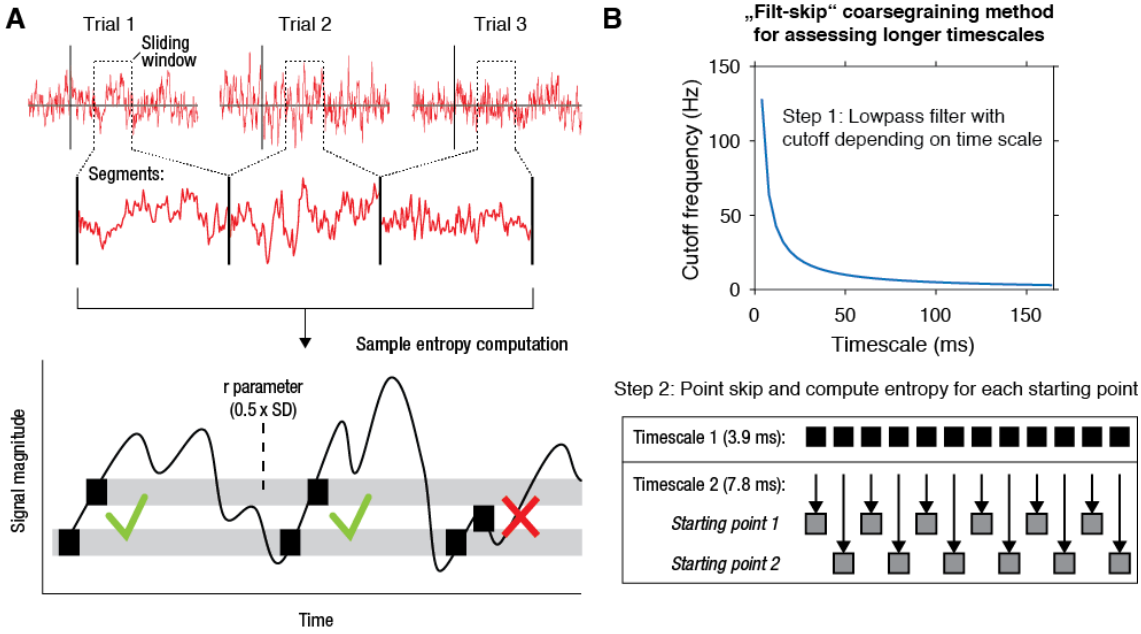

Figure 2 | mMSE estimation procedure. A. Discontinuous entropy computation procedure. Data segments of 0.5 s duration centered on a specific time point from each trial's onset (top row) are selected and concatenated (middle row). Entropy is then computed on this concatenated time series while excluding discontinuous segment borders by counting repeats of both m (here, m = 1 for illustration purposes) and m+1 (thus 2) sample patterns and taking the log ratio of the two pattern counts (bottom row). We used m = 2 in our actual analyses. The pattern similarity parameter r determines how lenient the algorithm is towards counting a pattern as a repeat by taking a proportion of the signal's standard deviation (SD), indicated by the width of the horizontal gray bars. The pattern counting procedure is repeated at each step of the sliding window, resulting in a time course of entropy estimates computed across trials. **B.** "Filt-skip" coarsegraining procedure used to estimate entropy on longer timescales, consisting of low-pass filtering followed by point-skipping. Filter cutoff frequency is determined by dividing the data sampling rate (here, 256 Hz i.e. 1 sample per 3.9 ms) by the index of the timescale of interest (top row). The signal is then coarsened by intermittently skipping samples (bottom row). In this example, every second sample is skipped at timescale 2, resulting in two different time courses depending on the starting point. Patterns are counted independently in both resulting time courses and summed before computing entropy.

bioRxiv preprint doi: https://doi.org/10.1101/834614; this version posted December 16, 2019. The copyright holder for this preprint (which was not certified by peer review) is the author/funder, who has granted bioRxiv a license to display the preprint in perpetuity. It is made available under aCC-BY-NC-ND 4.0 International license.

We tested for a relationship between shifts in decision bias and neural variability between the conservative and liberal conditions by Spearman-correlating joint modulations of mMSE and criterion across participants (averaged over the three sessions), for all electrodes, time points, and timescales. Strikingly, we found a negative cluster of correlations in mid- and left-frontal electrodes ($p = 0.022$, cluster-corrected for multiple comparisons (Maris and Oostenveld, 2007)) indicating that participants who showed a larger bias shift from the conservative to the liberal condition were those who also exhibited a larger boost in frontal entropy (Figure 3A). The cluster ranged across timescales from ~20-164 ms, with most of the cluster located after trial initialization (solid vertical line in Figure 3A). To illustrate this correlation, we averaged liberal–conservative mMSE within the significant cluster and plotted the across-participant change-change correlation (rho = –0.90) with criterion (Figure 3B).

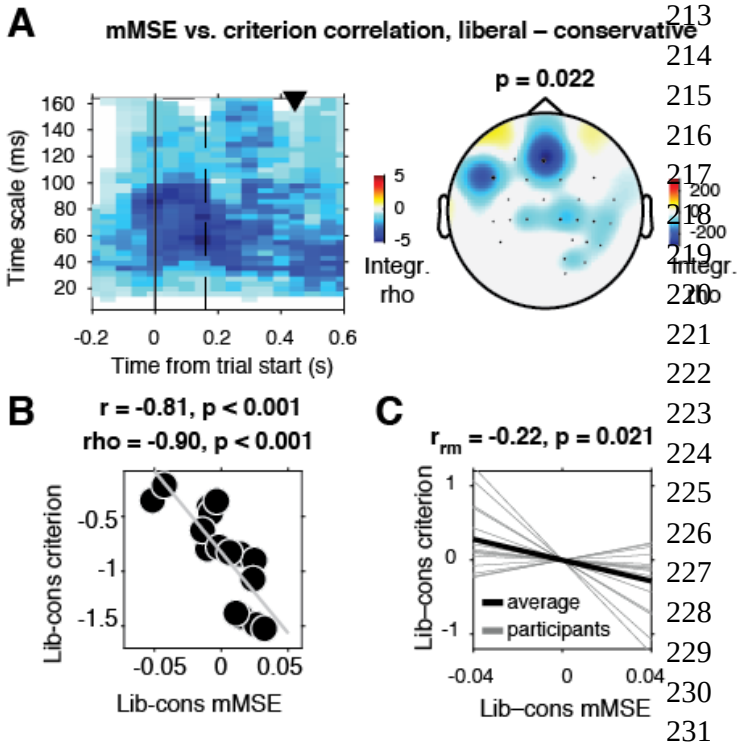

Figure 3 | **Change-change correlation between liberal–conservative shifts in mMSE and bias. A.** Significant negative electrode-time-timescale cluster observed via Spearman correlation between liberal–conservative mMSE and liberal–conservative SDT criterion. Correlations outside the significant cluster are masked out. Left, time-timescale representation showing the correlation cluster integrated over the electrodes indicated by the black circles in the topographical scalp map. The solid vertical line indicates the time of trial onset. The dotted vertical line indicates time of (non)target onset. Right, scalp map of mMSE integrated across significant time-timescale bins. P-value above scalp map indicates multiple comparison-corrected cluster significance using a permutation test across participants. **B.** Scatter plot of the correlation after averaging mMSE within the significant cluster. Both Pearson's r and Spearman's rho are indicated. **C.** Single-subject mMSE vs. criterion slopes across liberal–conservative block pairs. r_{rm}, repeated measures correlation across all block pairs performed after centering each subject's shifts in mMSE and criterion around zero.

The following source data and figure supplements are available for Figure 2:

Source data 1. This MATLAB file contains the data for Figure 3.

Figure supplement 1. Correlation between liberal – conservative mMSE and bias shift is reliable in split data halves.

Figure supplement 2. Change-change correlations between liberal–conservative mMSE, criterion, EEG signal SD and spectral power.

bioRxiv preprint doi: https://doi.org/10.1101/834614; this version posted December 16, 2019. The copyright holder for this preprint (which was not certified by peer review) is the author/funder, who has granted bioRxiv a license to display the preprint in perpetuity. It is made available under aCC-BY-NC-ND 4.0 International license.

Figure supplement 3. EEG spectral power normalized with respect to the pre-trial baseline.

We next employed several approaches to strengthen evidence for the observed link between shifts in neural variability and decision bias. First, we asked whether mMSE and bias were also linked within participants across the nine liberal–conservative block pairs (see Figure 1A, bottom and 1D). Critically, we observed a negative repeated measures correlation (Bakdash and Marusich, 2017) between within-participant shifts in criterion and mMSE (r_{rm} = –0.19, p = 0.039, Figure 3C), providing convergent within-person evidence for a link between shifts in decision bias and neural variability. Second, correlating across a relatively low number of observations can be unreliable (Yarkoni, 2009) depending on the amount of data underlying each observation. We therefore tested whether the correlation across participants was present within two separate halves of the data after an arbitrary split based on odd and even trials. We found significant correlations in both data halves, indicating reliable between-subject associations (odd, rho = –0.61, p = 0.013; even, rho = –0.64, p = 0.009, see Figure 3, figure supplement 1).

Third, we investigated whether the correlation could alternatively be explained by potential confounds. Specifically, entropy estimates can be influenced by the time-domain signal SD through the pattern similarity (r) parameter (see Figure 2), even when this parameter is recomputed for each timescale after coarsegraining, as done here (Kosciessa et al., 2019). In addition, E/MEG data is often quantified in terms of oscillatory spectral power in canonical delta (1-2 Hz), theta (3-7 Hz), alpha (8-12 Hz), beta (13-30 Hz) and gamma (60-100 Hz) bands (see Kloosterman et al. (Kloosterman et al., 2019) for detailed spectral analysis of the current dataset), which might be able to explain the entropy results through a similar dependency. Therefore, we tested whether the ∆bias-∆entropy correlation could be explained by broadband signal SD and band-specific spectral power. To make the computation of spectral power and entropy as similar as possible, we used the same 0.5 s sliding window and 50 ms step size for spectral analysis (1 s window to allow delta power estimation, see methods), and selected spectral power within the same electrodes and time points in which the mMSE effect was indicated. Strikingly, we found that the ∆bias-∆entropy correlation remained strong and significant both when controlling for signal SD (partial rho = –0.82, p < 0.0001), and even when controlling for all major power bands simultaneously (delta, theta, alpha, beta, gamma; partial rho = –0.68, p = 0.02). See Figure 3, figure supplement 2 for correlations between mMSE and various potentially confounding factors. Moreover, we found no significant clusters when correlating the bias shift with liberal–conservative spectral power modulation computed by normalizing spectral power using the pre-stimulus baseline, indicating that power modulation also does not track bias shifts (Figure 3, figure supplement 3). Interestingly, explicitly controlling for overall signal variation (SD) in each time-scale bin in each electrode via partial Spearman correlation narrowed the cluster of significant correlations down to timescales from 20-100 ms (Figure 4A), suggesting that the slower timescales implicated in the mMSE correlation in Figure 3A are primarily driven by overall signal variation rather than moment-to-moment variability,

bioRxiv preprint doi: https://doi.org/10.1101/834614; this version posted December 16, 2019. The copyright holder for this preprint (which was not certified by peer review) is the author/funder, who has granted bioRxiv a license to display the preprint in perpetuity. It is made available under aCC-BY-NC-ND 4.0 International license.

whereas intermediate timescales are more driven by moment-to-moment variability. Spatially, the SD-controlled correlation cluster more prominently involved temporal and occipital electrodes, suggesting involvement of sensory and association cortex. Importantly, the results did depend on our modified entropy estimation method, since the frontal correlation cluster was smaller and non-significant when performing the Δbias-Δentropy correlation using conventional MSE (cluster p = 0.37)(Costa et al., 2002)(Figure 4B). Note that we still employed our novel sliding window approach for comparison with the principal mMSE correlation analysis. Statistically controlling for the participants' perceptual ability to detect targets, quantified as the liberal–conservative shift in SDT sensitivity measure d' (Green and Swets, 1966) did not affect the relationship (partial rho = –0.88, p < 0.0001), indicating that perceptual sensitivity could not explain our results.

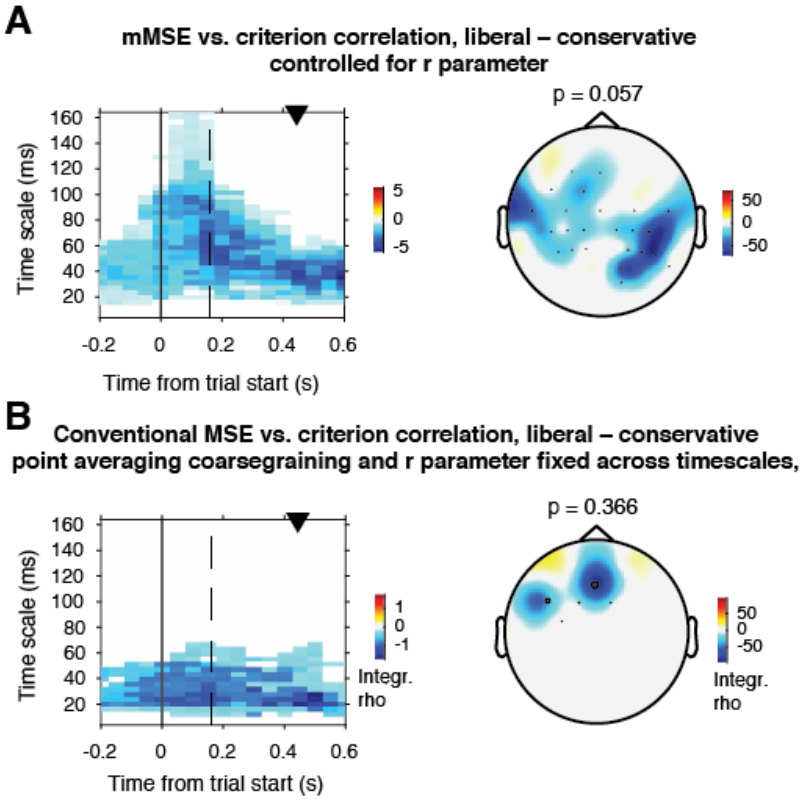

Figure 4 | A. Liberal – conservative mMSE vs. criterion correlation when statistically controlling for the r parameter (signal SD) across participants. The cluster remains significant and the topography is similar, but the effect is more widespread across electrodes, and less widespread across timescales. **B.** As A. but using traditional MSE, including coarse graining through point averaging to asses longer timescales and a fixed r parameter across timescales. The cluster does not reach significance.

Finally, improved perceptual sensitivity has been linked to a transient, post-stimulus decrease in neural variability, referred to as variability 'quenching' (Arazi et al., 2017; Churchland et al., 2010; Schurger et al., 2015). Quenching is directly predicted by attractor models of brain organization (Wang, 2002), and is consistent with SDT's main principle that suppression of neural noise enhances perception (Green and Swets, 1966). Quenching has also been reported in the human EEG in terms of a

bioRxiv preprint doi: https://doi.org/10.1101/834614; this version posted December 16, 2019. The copyright holder for this preprint (which was not certified by peer review) is the author/funder, who has granted bioRxiv a license to display the preprint in perpetuity. It is made available under aCC-BY-NC-ND 4.0 International license.

variance reduction across trials in visual cortex following stimulus onset (Arazi et al., 2017), although this type of quenching can be attributed to the well-known suppression of low-frequency spectral power following stimulus onset (Daniel et al., 2019). In the mMSE modulation with respect to prestimulus baseline we found both a midfrontal and lateral occipital and temporal enhancement of mMSE modulation (Figure 5A) that could not be explained by spectral power (Figure 5B), as well as an mMSE quenching cluster in shorter mMSE timescales (Figure 5C) that was significantly correlated with low-frequency (beta) power (Figure 5D). However, we found significant clusters neither when correlating liberal–conservative mMSE quenching with shifts in bias, nor with shifts in d'. Furthermore, controlling for signal SD (which is most strongly affected by low-frequency power due to the 1/f nature of EEG signals) completely abolished the mMSE quenching, again indicating that this effect could indeed be explained by low-frequency spectral power. When contrasting the conditions, we did find a significant positive cluster in midfrontal electrodes, indicating a stronger transient increase in entropy following trial onset in the liberal condition (Figure 5E). Finally, when change-change correlating mMSE and criterion, we found a left-lateralized negative cluster in temporal electrodes (Figure 5F). Taken together, these various control analyses suggest a unique contribution of moment-to-moment neural variability to bias shifts in human decision making, over and above overall brain signal variation, oscillatory neural dynamics, variability quenching, and perceptual sensitivity.

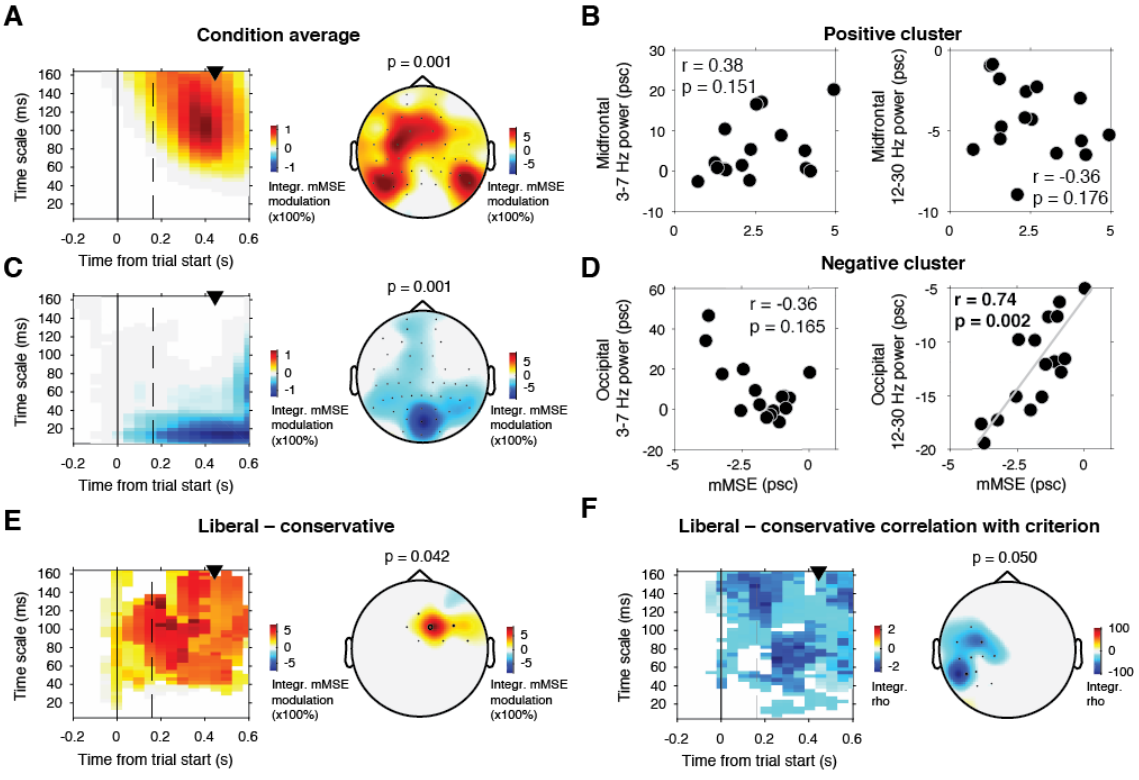

Figure 5 | mMSE modulation with respect to pre-trial baseline. A. Significant positive cluster observed in longer timescales after normalizing mMSE values to percent signal change (psc) units with respect to the pre-trial baseline (–0.2 to 0 s) and averaging across conditions. **B.** Correlation

bioRxiv preprint doi: https://doi.org/10.1101/834614; this version posted December 16, 2019. The copyright holder for this preprint (which was not certified by peer review) is the author/funder, who has granted bioRxiv a license to display the preprint in perpetuity. It is made available under aCC-BY-NC-ND 4.0 International license.

between mMSE modulation in the positive cluster depicted in A. and spectral power modulation in midfrontal electrodes. Left panel, 3-7 Hz; right panel, 12-30 Hz. **C. D.** As B. but for the posterior negative cluster. **E.** Significant positive cluster observed in mid-frontal electrodes in the liberal–conservative contrast of mMSE modulation. **F.** Significant cluster resulting from the correlation between liberal–conservative mMSE modulation with liberal–conservative SDT criterion. Conventions as in Figure 3.

Discussion

Strategic decision biases allow organisms to adapt their choices to the context in which decisions are made. Frontal cortex has previously been shown to be involved in strategic bias shifts in humans (Rahnev et al., 2016a) and monkeys (Ferrera et al., 2009), but its spatiotemporal neural signature has to date remained elusive. Here, we provide first evidence that flexible adjustment of moment-to-moment variability in frontal regions may underlie such strategic shifts in decision bias, independent of brain signal SD and oscillatory neural dynamics. The observed relationship between shifts in bias and neural variability in anterior brain regions complements our previous findings in the frequency domain that humans can intentionally control prestimulus 8–12 Hz (alpha) oscillatory power in posterior cortex to strategically bias decision making (Kloosterman et al., 2019). Notably, we previously observed increased oscillatory 2—6 Hz (theta) power in the liberal compared to the conservative condition in the same midfrontal electrodes implicated here in the Δbias-Δentropy correlation, but this theta power difference was not correlated with the bias shift. This suggests that the bias shift may be reflected both in low-frequency spectral power and entropy in midfrontal regions, but that only entropy is linked to the magnitude of the decision-maker's bias shift. One possible explanation for such a dissociation is that spectral power exclusively reflects the amplitude of the signal's oscillatory fluctuations while discarding its phase information. In contrast, entropy is sensitive to both variations in the magnitude as well as the phase of EEG signal fluctuations, since more frequent phase resets will result in a more irregular time-domain signal that will yield higher entropy. Moreover, whereas spectral analysis strictly assumes a sinusoidal waveform of EEG signal fluctuations (Cole and Voytek, 2017; Jones, 2016), entropy is agnostic to the shape of the waveforms present in the signal. Entropy thus provides a more unrestricted description of moment-to-moment fluctuations in neural activity that is highly predictive of decision bias shifts across participants in our data.

In contrast with the central idea in this study that neural variability facilitates cognition, previous work has suggested that a temporary stabilization of neural activity after stimulus onset ('quenching') is beneficial for perception (Arazi et al., 2017; Schurger et al., 2015). Although we also observed quenching after baseline-correcting mMSE, we found no evidence for a change-change relationship between quenching and decision bias or perceptual sensitivity. This suggests that in contrast to our finding that rising variability facilitates a strategic bias shift, the degree to which individuals quench is not related to behavior in our data. We note, however, that quenching and rising of neural variability should not be mutually exclusive

bioRxiv preprint doi: https://doi.org/10.1101/834614; this version posted December 16, 2019. The copyright holder for this preprint (which was not certified by peer review) is the author/funder, who has granted bioRxiv a license to display the preprint in perpetuity. It is made available under aCC-BY-NC-ND 4.0 International license.

concepts, but can in principle occur simultaneously if one considers the different timescales in which these phenomena seem to occur: shorter scales (< 40 ms) for quenching and longer scales (> 40 ms) for rising variability. Furthermore, the relations between quenching observed in neural spiking (Churchland et al., 2010), trial-by-trial variance of E/MEG (Arazi et al., 2017) and mMSE are currently unclear, and require further future investigation. Future studies could also explore how neural variability quenching and rising in different timescales are related to various aspects of decision making, such as perceptual sensitivity, different kinds of biases (Fleming et al., 2010; Talluri et al., 2018; Urai et al., 2019), but also confidence and metacognitive processes (Fleming and Dolan, 2012; Yeung and Summerfield, 2012). Finally, individual decision bias has also been linked to the magnitude of transient dilations of the eye's pupil (de Gee et al., 2017, 2014), also in relation to entropy of EEG (Waschke et al., 2019), suggesting that pupil-linked neuromodulation (Joshi et al., 2015) is possibly linked to decision bias through moment-to-moment neural variability. Further investigation of the relationship between neural variability and neuromodulation could prove fruitful to shed light on the mechanisms underlying higher-order cognitive function (Garrett et al., 2015).

Our results suggest that dynamic adjustment of neural variability in frontal regions is crucial for adaptive behavior. Based on our findings, we propose that heightened frontal entropy results from a more dynamic, irregular neural regime that enables an individual to be more prepared to process and act upon uncertain, yet task-relevant information. In the current study, variability (entropy) provides a theoretically driven quantification of the neural instantiation of human decision making (Marzen and DeDeo, 2017; Młynarski and Hermundstad, 2018). We argue that quantifying shifts in neural entropy could help elucidate the mechanisms allowing organisms to adapt to their environment and ultimately increase their chances of survival.

Materials and Methods

We report a novel analysis of a previously published dataset involving a target detection task during two different decision bias manipulations (Kloosterman et al., 2019).

Subjects Sixteen participants (eight females, mean age 24.1 years, ± 1.64) took part in the experiment, either for financial compensation (EUR 10 per hour) or in partial fulfillment of first year psychology course requirements. Each participant completed three experimental sessions on different days, each session lasting ca. 2 hours, including preparation and breaks. One participant completed only two sessions, yielding a total number of sessions across subjects of 47. Due to technical issues, for one session only data for the liberal condition was available. One participant was an author. All participants had normal or corrected-to-normal vision and were right handed. Participants provided written informed consent before the start of the

bioRxiv preprint doi: https://doi.org/10.1101/834614; this version posted December 16, 2019. The copyright holder for this preprint (which was not certified by peer review) is the author/funder, who has granted bioRxiv a license to display the preprint in perpetuity. It is made available under aCC-BY-NC-ND 4.0 International license.

experiment. All procedures were approved by the ethics committee of the University of Amsterdam.

Stimuli Stimuli consisted of a continuous semi-random rapid serial visual presentation (rsvp) of full screen texture patterns. The texture patterns consisted of line elements approx. 0.07° thick and 0.4° long in visual angle. Each texture in the rsvp was presented for 40 ms (i.e. stimulation frequency 25 Hz), and was oriented in one of four possible directions: 0°, 45°, 90° or 135°. Participants were instructed to fixate a red dot in the center of the screen. At random inter trial intervals (ITI's) sampled from a uniform distribution (ITI range 0.3 – 2.2 s), the rsvp contained a fixed sequence of 25 texture patterns, which in total lasted one second. This fixed sequence consisted of four stimuli preceding a (non-)target stimulus (orientations of 45°, 90°, 0°, 90° respectively) and twenty stimuli following the (non)-target (orientations of 0°, 90°, 0°, 90°, 0°, 45°, 0°, 135°, 90°, 45°, 0°, 135°, 0°, 45°, 90°, 45°, 90°, 135°, 0°, 135° respectively) (see Figure 1A). The fifth texture pattern within the sequence (occurring from 0.16 s after sequence onset) was either a target or a nontarget stimulus. Nontargets consisted of either a 45° or a 135° homogenous texture, whereas targets contained a central orientation-defined square of 2.42° visual angle, thereby consisting of both a 45° and a 135° texture. 50% of all targets consisted of a 45° square and 50% of a 135° square. Of all trials, 75% contained a target and 25% a nontarget. Target and nontarget trials were presented in random order. To avoid specific influences on target stimulus visibility due to presentation of similarly or orthogonally oriented texture patterns temporally close in the cascade, no 45° and 135° oriented stimuli were presented directly before or after presentation of the target stimulus. All stimuli had an isoluminance of 72.2 cd/m^2. Stimuli were created using MATLAB (The Mathworks, Inc., Natick, MA, USA) and presented using Presentation version 9.9 (Neurobehavioral systems, Inc., Albany, CA, USA).

Experimental design The participants' task was to detect and actively report targets by pressing a button using their right hand. Targets occasionally went unreported, presumably due to constant forward and backward masking by the continuous cascade of stimuli and unpredictability of target timing (Fahrenfort et al., 2007). The onset of the fixed order of texture patterns preceding and following (non-)target stimuli was neither signaled nor apparent. At the beginning of the experiment, participants were informed they could earn a total bonus of EUR 30, -, on top of their regular pay of EUR 10, - per hour or course credit. In two separate conditions within each session of testing, we encouraged participants to use either a conservative or a liberal bias for reporting targets using both aversive sounds as well as reducing their bonus after errors. In the conservative condition, participants were instructed to only press the button when they were relatively sure they had seen the target. The instruction on screen before block onset read as follows: 'Try to detect as many targets as possible. Only press when you are relatively sure you just saw a target.' To maximize effectiveness of this instruction, participants were told the bonus would be diminished by 10 cents after a false alarm. During the experiment, a loud aversive sound was played after a false alarm to inform the participant about an error. During

bioRxiv preprint doi: https://doi.org/10.1101/834614; this version posted December 16, 2019. The copyright holder for this preprint (which was not certified by peer review) is the author/funder, who has granted bioRxiv a license to display the preprint in perpetuity. It is made available under aCC-BY-NC-ND 4.0 International license.

the liberal condition, participants were instructed to miss as few targets as possible. The instruction on screen before block onset read as follows: 'Try to detect as many targets as possible. If you sometimes press when there was nothing this is not so bad'. In this condition, the loud aversive sound was played twice in close succession whenever they failed to report a target, and three cents were subsequently deducted from their bonus. The difference in auditory feedback between both conditions was included to inform the participant about the type of error (miss or false alarm), in order to facilitate the desired bias in both conditions. After every block, the participant's score (number of missed targets in the liberal condition and number of false alarms in the conservative condition) was displayed on the screen, as well as the remainder of the bonus. After completing the last session of the experiment, every participant was paid the full bonus as required by the ethical committee.

Participants performed six blocks per session lasting ca. nine minutes each. During a block, participants continuously monitored the screen and were free to respond by button press whenever they thought they saw a target. Each block contained 240 trials, of which 180 target and 60 nontarget trials. The task instruction was presented on the screen before the block started. The condition of the first block of a session was counterbalanced across participants. Prior to EEG recording in the first session, participants performed a 10-min practice run of both conditions, in which visual feedback directly after a miss (liberal condition) or false alarm (conservative) informed participants about their mistake, allowing them to adjust their decision bias accordingly. There were short breaks between blocks, in which participants indicated when they were ready to begin the next block.

Behavioral analysis We defined decision bias as the criterion measure from SDT (Green and Swets, 1966). We calculated the criterion *c* across the trials in each condition as follows:

$$c = -\frac{1}{2}\left[Z(Hit\text{-}rate) + Z(FA\text{-}rate)\right]$$

where hit-rate is the proportion target-present responses of all target-present trials, false alarm (FA)-rate is the proportion target-present responses of all target-absent trials, and Z(...) is the inverse standard normal distribution. Furthermore, we calculated perceptual sensitivity using the SDT measure d`:

$$d' = Z(Hit\text{-}rate) - Z(FA\text{-}rate)$$

EEG recording Continuous EEG data were recorded at 256 Hz using a 48-channel BioSemi Active-Two system (BioSemi, Amsterdam, the Netherlands), connected to a standard EEG cap according to the international 10-20 system. Electrooculography (EOG) was recorded using two electrodes at the outer canthi of the left and right eyes and two electrodes placed above and below the right eye. Horizontal and vertical EOG electrodes were referenced against each other, two for horizontal and two for vertical eye movements (blinks). We used the FieldTrip toolbox (Oostenveld

bioRxiv preprint doi: https://doi.org/10.1101/834614; this version posted December 16, 2019. The copyright holder for this preprint (which was not certified by peer review) is the author/funder, who has granted bioRxiv a license to display the preprint in perpetuity. It is made available under aCC-BY-NC-ND 4.0 International license.

et al., 2011) and custom software in MATLAB R2016b (The Mathworks Inc., Natick, MA, USA; RRID:SCR_001622) to process the data. Data were re-referenced to the average voltage of two electrodes attached to the earlobes. We applied a Butterworth high-pass filter (fourth order, cutoff 0.5 Hz) to remove slow drifts from the data.

Trial extraction We extracted trials of variable duration from 1 s before target sequence onset until 1.25 after button press for trials that included a button press (hits and false alarms), and until 1.25 s after stimulus onset for trials without a button press (misses and correct rejects). The following constraints were used to classify (non-)targets as detected (hits and false alarms), while avoiding the occurrence of button presses in close succession to target reports and button presses occurring outside of trials: 1) A trial was marked as detected if a response occurred within 0.84 s after target onset; 2) when the onset of the next target stimulus sequence started before trial end, the trial was terminated at the next trial's onset; 3) when a button press occurred in the 1.5 s before trial onset, the trial was extracted from 1.5 s after this button press; 4) when a button press occurred between 0.5 s before until 0.2 s after sequence onset, the trial was discarded. After trial extraction the mean of every channel was removed per trial.

Artifact rejection Trials containing muscle artifacts were rejected from further analysis using a standard semi-automatic preprocessing method in Fieldtrip. This procedure consists of bandpass-filtering the trials of a condition block in the 110–125 Hz frequency range, which typically contains most of the muscle artifact activity, followed by a Z-transformation. Trials exceeding a threshold Z-score were removed completely from analysis. We used as the threshold the absolute value of the minimum Z-score within the block, + 1. To remove eye blink artifacts from the time courses, the EEG data from a complete session were transformed using independent component analysis (ICA), and components due to blinks (typically one or two) were removed from the data. In addition, to remove microsaccade-related artifacts we included two virtual channels in the ICA based on channels Fp1 and Fp2, which included transient spike potentials as identified using the saccadic artefact detection algorithm from (Hassler et al., 2011). This yielded a total number of channels submitted to ICA of 48 + 2 = 50. The two components loading high on these virtual electrodes (typically with a frontal topography) were also removed. Blinks and eye movements were then semi-automatically detected from the horizontal and vertical EOG (frequency range 1–15 Hz; z-value cut-off 4 for vertical; 6 for horizontal) and trials containing eye artefacts within 0.1 s around target onset were discarded. This step was done to remove trials in which the target was not seen because the eyes were closed. Finally, trials exceeding a threshold voltage range of 200 mV were discarded. To attenuate volume conduction effects and suppress any remaining microsaccade-related activity, the scalp current density (SCD) was computed using the second-order derivative (the surface Laplacian) of the EEG potential distribution (Perrin et al., 1989).

bioRxiv preprint doi: https://doi.org/10.1101/834614; this version posted December 16, 2019. The copyright holder for this preprint (which was not certified by peer review) is the author/funder, who has granted bioRxiv a license to display the preprint in perpetuity. It is made available under aCC-BY-NC-ND 4.0 International license.

ERP removal We removed stimulus-evoked EEG activity related to external events by computing the event-related potential (ERP) and subtracting the ERP from each single trial prior to entropy or spectral analysis. This was done to focus on ongoing (termed “induced”, (Klimesch et al., 1998)) activity and eliminate large-amplitude transients from the data that would increase the signal standard deviation and thus affect the r parameter that is used for determining pattern matches. To eliminate differences in evoked responses between sessions and conditions, we performed this procedure separately for ERPs computed in each condition, session, and participant.

Entropy computation We measured temporal neural variability in the EEG using multiscale entropy (MSE) (Costa et al., 2002). MSE characterizes signal irregularity at multiple time scales by estimating sample entropy (SampEn) at each time scale of interest. The estimation of SampEn involves counting how often patterns of m successive data points reoccur in time (p^m) and assessing how many of those patterns remain similar when the next sample m+1 is added to the sequence (p^(m+1)). Given that amplitude values are rarely exactly equal in physiological time series, a similarity bound defines which individual data points are considered similar. This step discretizes the data and allows to compare data patterns rather than exact data values. The similarity bound is defined as a proportion r of the time series standard deviation (SD; i.e., square root of signal variance) to normalize the estimation of sample entropy for total signal variation. That is, for any data point k, all data points within k□±□r□×□SD are by definition equal to k, which forms the basis for assessing sequence patterns. SampEn is finally given as the natural log of p^m(r)/ p^(m+1)(r). Consequently, high SampEn values indicate low temporal regularity as many patterns of length m are not repeated at length m+1. In our applications, m was set to 2 and r was set to .5, in line with prior recommendations (Richman and Moorman, 2000) and EEG applications (Courtiol et al., 2016; Heisz and McIntosh, 2013; Kosciessa et al., 2019; McIntosh et al., 2008).

Discontinuous MSE computation An important limitation of MSE is the need for substantial continuous data for robust estimation. Heuristically, the recommended number of successive data points for estimation at each scale is 100 (minimum) to 900 (preferred) points using typical MSE parameter settings (Grandy et al., 2016). This limitation precludes the application of MSE to neuroimaging data recorded during cognitive processes that unfold over brief periods of time, such as perceptual decisions. Grandy et al. (Grandy et al., 2016) showed that the pattern counting process can be extended to discontinuous data segments that are concatenated across time, as long as the counting of artificial patterns across segment borders is avoided (as these patterns are a product of the concatenation and do not occur in the data itself). We applied the MSE computation across discontinuous segments of 0.5 s duration (window size). To track the evolution of MSE over the trial, we slid this window across the trials in steps of 50 milliseconds from -0.2 s until 0.6 s, each time recomputing MSE across segments taken from the time window in each trial.

bioRxiv preprint doi: https://doi.org/10.1101/834614; this version posted December 16, 2019. The copyright holder for this preprint (which was not certified by peer review) is the author/funder, who has granted bioRxiv a license to display the preprint in perpetuity. It is made available under aCC-BY-NC-ND 4.0 International license.

Multi-scale implementation through time series coarsegraining By counting the reoccurrences of patterns of adjacent data points, SampEn measures entropy at the time scale of the signal's sampling rate, which is in the order of milliseconds or shorter in EEG data. To enable estimation of entropy at longer time scales, the time series is typically coarsegrained by averaging groups of adjacent samples ('point averaging') and repeating the entropy computation (Costa et al., 2002). However, despite its simplicity, this method is suboptimal for eliminating short temporal scales. Point averaging is equivalent to low-pass filtering using a finite-impulse response filter, which does not effectively eliminate higher frequencies and can introduce aliasing (Semmlow, 2004; Valencia et al., 2009). For this reason, an improved coarse graining procedure was introduced involving replacement of the multi-point average by a low-pass Butterworth filter, which has a well-defined frequency cutoff and precludes aliasing (Valencia et al., 2009)(Figure 2B, top). The filter cutoff frequency is determined by the ratio of 1 and the scale number, such that an increasingly larger portion of the higher frequencies is removed for slower time scales. Notably, low-pass filtering affects the temporal structure of the time-domain signal, which could hamper the interpretation of the EEG dynamics due to smearing of responses (VanRullen, 2011). This issue is largely mitigated, however, due to the liberal–conservative subtraction that we perform before correlating with behavior, since this issue presumably affects both conditions similarly. Filtering is followed by a point-skipping procedure to reduce the signal's sampling rate (Figure 2B, bottom). Since point-skipping omits increasingly large portions of the filtered time series depending on the starting point of the point-skipping procedure, we counted patterns separately for each starting point within a scale, summed their counts for two-point and three-point matches separately and computed entropy as described above. Given our segments of 0.5 s window length sampled at 256 Hz, we computed MSE for scales 1 (129 samples within the window) until 42 (three or four samples within the window, depending on the starting point). Note that using a pattern parameter of $m = 2$, a minimum of three samples within a segment is required to estimate entropy across the segments of continuous data, yielding a maximum possible scale of 42. In line with the MSE literature (Courtiol et al., 2016), we converted the time scale units to milliseconds by taking the duration between adjacent data points after each coarsegraining step. For example, time scale 1 corresponds to 1000 ms / 256 Hz = 3.9 ms, and scale 42 to 1000 / (256/42) = 164 ms.

Pattern similarity parameter computation at each time scale By increasingly smoothing the time series, coarse-graining affects not only on the signal's entropy, but also its overall variation, as reflected in the decreasing standard deviation as a function of time scale (Nikulin and Brismar, 2004). In the original implementation of the MSE calculation, the similarity parameter r was set as a proportion of the original (scale 1) time series' standard deviation and applied to all the scales (Costa et al., 2002). Because of the decreasing variation in the time series due to coarse graining, the similarity parameter therefore becomes increasingly tolerant at slower time scales, resulting in more similar patterns and decreased entropy. This decreasing

bioRxiv preprint doi: https://doi.org/10.1101/834614; this version posted December 16, 2019. The copyright holder for this preprint (which was not certified by peer review) is the author/funder, who has granted bioRxiv a license to display the preprint in perpetuity. It is made available under aCC-BY-NC-ND 4.0 International license.

entropy can be attributed both to changes in signal complexity, but also in overall variation (Kosciessa et al., 2019; Nikulin and Brismar, 2004). To overcome this limitation, we recomputed the similarity parameter for each scale, thereby normalizing MSE with respect to changes in overall time series variation at each scale.

Spectral analysis We used a sliding window Fourier transform; step size, 50 ms; window size, 500 ms; frequency resolution, 2 Hz) to calculate time-frequency representations (spectrograms) of the EEG power for each electrode and each trial. We used a single Hann taper for the frequency range of 3–35 Hz (spectral smoothing, 4.5 Hz, bin size, 1 Hz) and the multitaper technique for the 36 – 100 Hz frequency range (spectral smoothing, 8 Hz; bin size, 2 Hz; five tapers)(Mitra and Bokil, 2007). See (Kloosterman et al., 2019) for similar settings. Finally, to investigate spectral power between 1-3 Hz (delta band), we performed an additional time-frequency analysis with a window size of 1 s (i.e. frequency resolution 1 Hz) without spectral smoothing (bin size 0.5 Hz). Spectrograms were aligned to the onset of the stimulus sequence containing the (non)target. Power modulations during the trials were quantified as the percentage of power change at a given time point and frequency bin, relative to a baseline power value for each frequency bin. We used as a baseline the mean EEG power in the interval 0.4 to 0 s before trial onset, computed separately for each condition. If this interval was not completely present in the trial due to preceding events (see Trial extraction), this period was shortened accordingly. We normalized the data by subtracting the baseline from each time-frequency bin and dividing this difference by the baseline (x 100 %).

Statistical significance testing of EEG power modulations and correlations across space, time and timescale/frequency. To determine clusters of significant modulation with respect to the pre-stimulus baseline without any a priori selection, we ran statistics across space-time-frequency bins using paired t-tests across subjects performed at each bin. Single bins were subsequently thresholded at $p < 0.05$ and clusters of contiguous time-space-frequency bins were determined. For the correlation versions of this analysis, we correlated the brain measure at each bin with the criterion and converted the r-values to a t-statistic using the Fisher-transformation (Fisher, 1915). We used a cluster-based procedure (Maris and Oostenveld, 2007) to correct for multiple comparisons using a cluster-formation alpha of $p < 0.05$ and a cluster-corrected alpha of $p = 0.05$, two-tailed. For visualization purposes, we integrated (using MATLAB's trapz function) power or entropy values in the time-frequency/entropy representations (TFR/TTR) across the highlighted electrodes in the topographies. For the topographical scalp maps, modulation was integrated across the saturated time-frequency bins in the TFRs/TTRs. See (Kloosterman et al., 2019) for a similar procedure in the time-frequency domain.

Correlation analysis We used both Pearson correlation and robust Spearman correlation across participants to test the relationships between the behavioral

bioRxiv preprint doi: https://doi.org/10.1101/834614; this version posted December 16, 2019. The copyright holder for this preprint (which was not certified by peer review) is the author/funder, who has granted bioRxiv a license to display the preprint in perpetuity. It is made available under aCC-BY-NC-ND 4.0 International license.

variables as well as with the EEG entropy and power (modulation). To test whether behavior and EEG activity were linked within participants, we used repeated measures correlation. Repeated measures correlation determines the common within-individual association for paired measures assessed on two or more occasions for multiple individuals by controlling for the specific range in which individuals' measurements operate, and correcting the correlation degrees of freedom for non-independence of repeated measurements obtained from each individual (Bakdash and Marusich, 2017; Bland and Altman, 1995). To test whether spectral power could account for the observed correlation between criterion and mMSE, we used partial Spearman and Pearson correlation controlling for other variables.

Data and code sharing The data analyzed in this study are publicly available on Figshare (Kloosterman et al., 2018). We programmed mMSE analysis in a MATLAB function within the format of the FieldTrip toolbox (Oostenveld et al., 2011). Our ft_entropyanalysis.m function takes as input data produced by Fieldtrip's ft_preprocessing.m function. In our function, we employed matrix computation of mMSE for increased speed, which is desirable due to the increased computational demand with multi-channel data analyzed with a sliding window. The function supports GPU functionality to further speed up computations. The function is available online (https://github.com/LNDG/mMSE).

Acknowledgments: Funding: Emmy Noether Grant to Douglas D Garrett, Max Planck UCL Centre for Computational Psychiatry and Ageing Research to Douglas Garrett, Niels Kloosterman, and Max Planck Society. **Author contributions:** Niels Kloosterman, Conceptualization, Data curation, Software, Formal analysis, Investigation, Visualization, Methodology, Writing—original draft, Project administration, Writing—review and editing; Julian Kosciessa, Software, Formal analysis, Writing—review and editing; Ulman Lindenberger, Resources, Funding acquisition, Writing—review and editing; Johannes Jacobus Fahrenfort, Conceptualization, Data curation, Software, Formal analysis, Supervision, Visualization, Methodology, Writing—original draft, Project administration, Writing—review and editing; Douglas Garrett, Conceptualization, Resources, Formal analysis, Supervision, Funding acquisition, Investigation, Methodology, Writing—review and editing. **Competing interests:** Authors declare no competing interests. **Data and materials availability:** All data analyzed during this study are publicly available (Kloosterman et al., 2018). Analysis scripts are publicly available on Github (https://github.com/kloosterman/critEEGentropy, https://github.com/LNDG/mMSE). A tutorial for computing mMSE within the FieldTrip toolbox has been published on the FieldTrip website (http://www.fieldtriptoolbox.org/example/entropy_analysis/).

References

bioRxiv preprint doi: https://doi.org/10.1101/834614; this version posted December 16, 2019. The copyright holder for this preprint (which was not certified by peer review) is the author/funder, who has granted bioRxiv a license to display the preprint in perpetuity. It is made available under aCC-BY-NC-ND 4.0 International license.

Arazi A, Censor N, Dinstein I. 2017. Neural Variability Quenching Predicts Individual Perceptual Abilities. *J Neurosci* **37**:97 109. doi:10.1523/jneurosci.1671-16.2017

Bakdash JZ, Marusich LR. 2017. Repeated Measures Correlation. *Front Psychol* **8**:491. doi:10.3389/fpsyg.2017.00456

Bland MJ, Altman DG. 1995. Statistics notes: Calculating correlation coefficients with repeated observations: Part 1—correlation within subjects. *Bmj* **310**:446 446. doi:10.1136/bmj.310.6977.446

Chen M-Y, Jimura K, White CN, Maddox TW, Poldrack RA. 2015a. Multiple brain networks contribute to the acquisition of bias in perceptual decision-making. *Front Neurosci-switz* **9**:63. doi:10.3389/fnins.2015.00063

Chen M-Y, Jimura K, White CN, Maddox TW, Poldrack RA. 2015b. Multiple brain networks contribute to the acquisition of bias in perceptual decision-making. *Front Neurosci-switz* **9**:63. doi:10.3389/fnins.2015.00063

Churchland MM, Yu BM, Cunningham JP, Sugrue LP, Cohen MR, Corrado GS, Newsome WT, Clark AM, Hosseini P, Scott BB, Bradley DC, Smith MA, Kohn A, Movshon AJ, Armstrong KM, Moore T, Chang SW, Snyder LH, Lisberger SG, Priebe NJ, Finn IM, Ferster D, Ryu SI, Santhanam G, Sahani M, Shenoy KV. 2010. Stimulus onset quenches neural variability: a widespread cortical phenomenon. *Nat Neurosci* **13**:369 378. doi:10.1038/nn.2501

Cole SR, Voytek B. 2017. Brain Oscillations and the Importance of Waveform Shape. *Trends Cogn Sci* **21**:137–149. doi:10.1016/j.tics.2016.12.008

Costa M, Goldberger AL, Peng C-K. 2002. Multiscale entropy analysis of complex physiologic time series. *Phys Rev Lett* **89**:068102. doi:10.1103/physrevlett.89.068102

Courtiol J, Perdikis D, Petkoski S, Müller V, Huys R, Sleimen-Malkoun R, Jirsa VK. 2016. The multiscale entropy: Guidelines for use and interpretation in brain signal analysis. *J Neurosci Meth* **273**:175 190. doi:10.1016/j.jneumeth.2016.09.004

Daniel E, Meindertsma T, Arazi A, Donner TH, Dinstein I. 2019. The Relationship between Trial-by-Trial Variability and Oscillations of Cortical Population Activity. *Sci Rep-uk* **9**:16901. doi:10.1038/s41598-019-53270-7

de Gee J, Colizoli O, Kloosterman NA, Knapen T, Nieuwenhuis S, Donner TH. 2017. Dynamic modulation of decision biases by brainstem arousal systems. *Elife* **6**:309. doi:10.7554/elife.23232

de Gee J, Knapen T, Donner TH. 2014. Decision-related pupil dilation reflects upcoming choice and individual bias. *Proc National Acad Sci* **111**:E618 25. doi:10.1073/pnas.1317557111

Fahrenfort J, Scholte H, Lamme V. 2007. Masking disrupts reentrant processing in

bioRxiv preprint doi: https://doi.org/10.1101/834614; this version posted December 16, 2019. The copyright holder for this preprint (which was not certified by peer review) is the author/funder, who has granted bioRxiv a license to display the preprint in perpetuity. It is made available under aCC-BY-NC-ND 4.0 International license.

772 human visual cortex. *Journal of Cognitive Neuroscience* **19**:1488 1497.
773 doi:10.1162/jocn.2007.19.9.1488&url_ctx_fmt=info:ofi/fmt:kev:mtx:ctx&rft_val_fmt=inf
774 o:ofi/fmt:kev:mtx:journal&rft.atitle=masking
775
776 Ferrera VP, Yanike M, Cassanello C. 2009. Frontal eye field neurons signal changes
777 in decision criteria. *Nat Neurosci* **12**:1458 1462. doi:10.1038/nn.2434
778
779 Fisher R. 1915. Frequency Distribution of the Values of the Correlation Coefficient in
780 Samples from an Indefinitely Large Population. *Biometrika* **10**:507.
781 doi:10.2307/2331838
782
783 Fleming SM, Dolan RJ. 2012. The neural basis of metacognitive ability. *Philosophical*
784 *Transactions Royal Soc B Biological Sci* **367**:1338–1349.
785 doi:10.1098/rstb.2011.0417
786
787 Fleming SM, Thomas CL, Dolan RJ. 2010. Overcoming status quo bias in the human
788 brain. *Proc National Acad Sci* **107**:6005–6009. doi:10.1073/pnas.0910380107
789
790 Garrett DD, Kovacevic N, McIntosh AR, Grady CL. 2011. The importance of being
791 variable. *J Neurosci* **31**:4496 4503. doi:10.1523/jneurosci.5641-10.2011
792
793 Garrett DD, Nagel IE, Preuschhof C, Burzynska AZ, Marchner J, Wiegert S,
794 Jungehülsing GJ, Nyberg L, Villringer A, Li S-C, Heekeren HR, Bäckman L,
795 Lindenberger U. 2015. Amphetamine modulates brain signal variability and working
796 memory in younger and older adults. *Proc National Acad Sci* **112**:7593–7598.
797 doi:10.1073/pnas.1504090112
798
799 Garrett DD, Samanez-Larkin GR, Macdonald SW, Lindenberger U, McIntosh AR,
800 Grady CL. 2013. Moment-to-moment brain signal variability: A next frontier in human
801 brain mapping? *Neurosci Biobehav Rev* **37**:610 624.
802 doi:10.1016/j.neubiorev.2013.02.015
803
804 Grandy TH, Garrett DD, Schmiedek F, Werkle-Bergner M. 2016. On the estimation
805 of brain signal entropy from sparse neuroimaging data. *Sci Rep-uk* **6**:23073.
806 doi:10.1038/srep23073
807
808 Green D, Swets J. 1966. Signal detection theory and psychophysics. *Society* **1**:521.
809
810 Heisz JJ, McIntosh AR. 2013. Applications of EEG Neuroimaging Data: Event-
811 related Potentials, Spectral Power, and Multiscale Entropy. *J Vis Exp Jove* 50131.
812 doi:10.3791/50131
813
814 Jones SR. 2016. When brain rhythms aren't 'rhythmic': implication for their
815 mechanisms and meaning. *Curr Opin Neurobiol* **40**:72–80.
816 doi:10.1016/j.conb.2016.06.010
817
818 Joshi S, Li Y, Kalwani RM, Gold JI. 2015. Relationships between Pupil Diameter and
819 Neuronal Activity in the Locus Coeruleus, Colliculi, and Cingulate Cortex. *Neuron*
820 **0**:221 234. doi:10.1016/j.neuron.2015.11.028
821

bioRxiv preprint doi: https://doi.org/10.1101/834614; this version posted December 16, 2019. The copyright holder for this preprint (which was not certified by peer review) is the author/funder, who has granted bioRxiv a license to display the preprint in perpetuity. It is made available under aCC-BY-NC-ND 4.0 International license.

822 Klimesch W, Russegger H, ppelmayr, Pachinger T. 1998. A method for the
823 calculation of induced band power: implications for the significance of brain
824 oscillations. *Electroencephalogr Clin Neurophysiology Evoked Potentials Sect*
825 **108**:123 130. doi:10.1016/s0168-5597(97)00078-6
826
827 Kloosterman NA, de Gee J, Werkle-Bergner M, Lindenberger U, Garrett D,
828 Fahrenfort J. 2018. Data from: Humans strategically shift decision bias by flexibly
829 adjusting sensory evidence accumulation in visual cortex.
830 doi:https://doi.org/10.6084/m9.figshare.6142940
831
832 Kloosterman NA, de Gee J, Werkle-Bergner M, Lindenberger U, Garrett DD,
833 Fahrenfort J. 2019. Humans strategically shift decision bias by flexibly adjusting
834 sensory evidence accumulation. *Elife* **8**:e37321. doi:10.7554/elife.37321
835
836 Kosciessa JQ, Kloosterman NA, Garrett DD. 2019. Standard multiscale entropy
837 reflects spectral power at mismatched temporal scales: What's signal irregularity got
838 to do with it? *Biorxiv* 752808. doi:10.1101/752808
839
840 Maris E, Oostenveld R. 2007. Nonparametric statistical testing of EEG- and MEG-
841 data. *J Neurosci Meth* **164**:177–190. doi:10.1016/j.jneumeth.2007.03.024
842
843 Marzen SE, DeDeo S. 2017. The evolution of lossy compression. *J Roy Soc*
844 *Interface* **14**:20170166. doi:10.1098/rsif.2017.0166
845
846 McIntosh A, Kovacevic N, Itier RJ. 2008. Increased Brain Signal Variability
847 Accompanies Lower Behavioral Variability in Development. *Plos Comput Biol*
848 **4**:e1000106. doi:10.1371/journal.pcbi.1000106
849
850 Mitra P, Bokil H. 2007. Observed Brain Dynamics - Partha Mitra, Hemant Bokil -
851 Google Books.
852
853 Młynarski WF, Hermundstad AM. 2018. Adaptive coding for dynamic sensory
854 inference. *Elife* **7**:e32055. doi:10.7554/elife.32055
855
856 Nikulin VV, Brismar T. 2004. Comment on "Multiscale entropy analysis of complex
857 physiologic time series". *Phys Rev Lett* **92**:089803 author reply 089804.
858 doi:10.1103/physrevlett.92.089803
859
860 Oostenveld R, Fries P, Maris E, Schoffelen J-M. 2011. FieldTrip: open source
861 software for advanced analysis of MEG, EEG, and invasive electrophysiological
862 data. *Comput Intel Neurosc* **2011**:1 9. doi:10.1155/2011/156869
863
864 Perrin F, Pernier J, Bertrand O, Echallier J. 1989. Spherical splines for scalp
865 potential and current density mapping. *Electroen Clin Neuro* **72**:184 187.
866 doi:10.1016/0013-4694(89)90180-6
867
868 Rahnev D, Nee D, Riddle J, Larson A, D'Esposito M. 2016a. Causal evidence for
869 frontal cortex organization for perceptual decision making. *Proc National Acad Sci*
870 **113**:6059–6064. doi:10.1073/pnas.1522551113
871

bioRxiv preprint doi: https://doi.org/10.1101/834614; this version posted December 16, 2019. The copyright holder for this preprint (which was not certified by peer review) is the author/funder, who has granted bioRxiv a license to display the preprint in perpetuity. It is made available under aCC-BY-NC-ND 4.0 International license.

872 Rahnev D, Nee D, Riddle J, Larson A, D'Esposito M. 2016b. Causal evidence for
873 frontal cortex organization for perceptual decision making. *Proc National Acad Sci*
874 **113**:6059–6064. doi:10.1073/pnas.1522551113
875
876 Reckless GE, Ousdal OT, Server A, Walter H, Andreassen OA, Jensen J. 2014a.
877 The left inferior frontal gyrus is involved in adjusting response bias during a
878 perceptual decision making task. *Brain Behav* **4**:398–407. doi:10.1002/brb3.223
879
880 Reckless GE, Ousdal OT, Server A, Walter H, Andreassen OA, Jensen J. 2014b.
881 The left inferior frontal gyrus is involved in adjusting response bias during a
882 perceptual decision making task. *Brain Behav* **4**:398–407. doi:10.1002/brb3.223
883
884 Richman JS, Moorman RJ. 2000. Physiological time-series analysis using
885 approximate entropy and sample entropy. *Phys Rev A* **278**:H2039 H2049.
886 doi:10.1103/physreva.29.975
887
888 Schurger A, Sarigiannidis I, Naccache L, Sitt JD, Dehaene S. 2015. Cortical activity
889 is more stable when sensory stimuli are consciously perceived. *Proc National Acad*
890 *Sci* **112**:E2083–E2092. doi:10.1073/pnas.1418730112
891
892 Semmlow J. 2004. Signal Processing and Communications **22**.
893 doi:10.1201/9780203024058
894
895 Talluri B, Urai AE, Tsetsos K, Usher M, Donner TH. 2018. Confirmation Bias through
896 Selective Overweighting of Choice-Consistent Evidence. *Curr Biol* **28**.
897 doi:10.1016/j.cub.2018.07.052
898
899 Urai AE, de Gee J, Tsetsos K, Donner TH. 2019. Choice history biases subsequent
900 evidence accumulation. *Elife* **8**:e46331. doi:10.7554/elife.46331
901
902 Valencia J, Porta A, Vallverdu M, Claria F, Baranowski R, Orłowska-Baranowska E,
903 Caminal P. 2009. Refined multiscale entropy: application to 24-h Holter recordings of
904 heart period variability in healthy and aortic stenosis subjects. *Ieee T Bio-med Eng*
905 **56**:2202 2213. doi:10.1109/tbme.2009.2021986
906
907 VanRullen R. 2011. Four Common Conceptual Fallacies in Mapping the Time
908 Course of Recognition. *Front Psychol* **2**:365. doi:10.3389/fpsyg.2011.00365
909
910 Wang X-J. 2002. Probabilistic Decision Making by Slow Reverberation in Cortical
911 Circuits. *Neuron* **36**:955–968. doi:10.1016/s0896-6273(02)01092-9
912
913 Waschke L, Tune S, Obleser J. 2019. Local cortical desynchronization and pupil-
914 linked arousal differentially shape brain states for optimal sensory performance. *Elife*
915 **8**:e51501. doi:10.7554/elife.51501
916
917 Windmann S, Urbach TP, Kutas M. 2002a. Cognitive and Neural Mechanisms of
918 Decision Biases in Recognition Memory. *Cereb Cortex* **12**:808–817.
919 doi:10.1093/cercor/12.8.808
920
921 Windmann S, Urbach TP, Kutas M. 2002b. Cognitive and Neural Mechanisms of

bioRxiv preprint doi: https://doi.org/10.1101/834614; this version posted December 16, 2019. The copyright holder for this preprint (which was not certified by peer review) is the author/funder, who has granted bioRxiv a license to display the preprint in perpetuity. It is made available under aCC-BY-NC-ND 4.0 International license.

922 Decision Biases in Recognition Memory. *Cereb Cortex* **12**:808–817.
923 doi:10.1093/cercor/12.8.808
924
925 Yarkoni T. 2009. Big Correlations in Little Studies: Inflated fMRI Correlations Reflect
926 Low Statistical Power-Commentary on Vul et al. (2009). *Perspect Psychol Sci* **4**:294
927 298. doi:10.1111/j.1745-6924.2009.01127.x
928
929 Yeung N, Summerfield C. 2012. Metacognition in human decision-making:
930 confidence and error monitoring. *Philosophical Transactions Royal Soc B Biological*
931 *Sci* **367**:1310–1321. doi:10.1098/rstb.2011.0416
932